The EMBO Journal Vol.16 No.17 pp.5151–5161, 1997

X-ray structure of antistasin at 1.9 Å resolution and its modelled complex with blood coagulation factor Xa

Risto Lapatto[1], Ute Krengel, Herman A.Schreuder[2], Anita Arkema, Bijtske de Boer, Kor H.Kalk, Wim G.J.Hol[3], Peter D.J.Grootenhuis[4], John W.M.Mulders[4], Rein Dijkema[4], Henri J.M.Theunissen[4] and Bauke W.Dijkstra[5]

Laboratory of Biophysical Chemistry and BIOSON Research Institute, Department of Chemistry, University of Groningen, Nijenborgh 4, 9747 AG Groningen, The Netherlands and [4]Scientific Development Group, N.V. Organon, PO Box 20, 5340 BH Oss, The Netherlands

[1]Present address: Children's Hospital and Institute of Biomedicine, University of Helsinki, 00014 Helsinki, Finland
[2]Present address: Hoechst Aktiengesellschaft, 65926 Frankfurt am Main, Germany
[3]Present address: Department of Biological Structure and Howard Hughes Medical Institute, University of Washington, Box 357742, Seattle, WA 98195, USA

[5]Corresponding author

The three-dimensional structure of antistasin, a potent inhibitor of blood coagulation factor Xa, from the Mexican leech *Haementeria officinalis* was determined at 1.9 Å resolution by X-ray crystallography. The structure reveals a novel protein fold composed of two homologous domains, each resembling the structure of hirustasin, a related 55-residue protease inhibitor. However, hirustasin has a different overall shape than the individual antistasin domains, it contains four rather than two β-strands, and does not inhibit factor Xa. The two antistasin domains can be subdivided into two similarly sized subdomains with different relative orientations. Consequently, the domain shapes are different, the N-terminal domain being wedge-shaped and the C-terminal domain flat. Docking studies suggest that differences in domain shape enable the N-terminal, but not C-terminal, domain of antistasin to bind and inhibit factor Xa, even though both have a very similar reactive site. Furthermore, a putative exosite binding region could be defined in the N-terminal domain of antistasin, comprising residues 15–17, which is likely to interact with a cluster of positively charged residues on the factor Xa surface (Arg222/Lys223/Lys224). This exosite binding region explains the specificity and inhibitory potency of antistasin towards factor Xa. In the C-terminal domain of antistasin, these exosite interactions are prevented due to the different overall shape of this domain.

Keywords: antistasin/crystal structure/factor Xa/protease inhibitor/thrombosis

Introduction

Blood coagulation proceeds through the sequential activation of a number of plasma serine proteases, ultimately resulting in the formation of fibrin, an insoluble protein that is a major component of blood clots. Coagulation factor Xa plays an important role in this cascade of events, since it converts the zymogen prothrombin into thrombin, the enzyme that catalyses the formation of fibrin from fibrinogen. Furthermore, factor Xa cleaves and hence activates other components of the coagulation cascade, including factors V, VII, VIII and IX (see Padmanabhan *et al.*, 1993 for references).

Inhibitors of factor Xa might be used as drugs for the treatment and prevention of thrombosis, a pathological condition in which blood coagulation occurs in an uncontrolled manner (Mao, 1993). It has been reported that antistasin, a potent reversible inhibitor of factor Xa, displays antithrombotic activity in various *in vivo* models of venous and arterial thrombosis (Nutt *et al.*, 1991; Vlasuk *et al.*, 1991; Dunwiddie *et al.*, 1992a; Mellott *et al.*, 1992; Hauptmann and Kaiser, 1993). Apart from its anticoagulant activity, antistasin is able to suppress metastasis, possibly also via inhibition of factor Xa (Tuszinsky *et al.*, 1987). It is this antimetastatic property from which antistasin obtained its name. Originally, antistasin was isolated from the salivary glands of the Mexican leech, *Haementeria officinalis*, but since then, it has been cloned into eukaryotic expression vectors and overexpressed (Han *et al.*, 1989; Nutt *et al.*, 1991; Theunissen *et al.*, 1994). The purified protein has an inhibition constant for factor Xa of approximately 5×10^{-10} M and displays competitive, slow-tight binding inhibition characteristics (Dunwiddie *et al.*, 1989). Antistasin is rather selective for factor Xa: it hardly inhibits other serine proteases such as thrombin, chymotrypsin, pancreatic elastase and leukocyte elastase (Dunwiddie *et al.*, 1989).

Antistasin is a small, disulfide cross-linked protein of 119 amino acid residues (M_r = 15 kDa). Figure 1 shows a comparison of its amino acid sequence with the sequences of the related proteinase inhibitors ghilanten and hirustasin. Ghilanten is a factor Xa inhibitor isolated from the salivary glands of the Amazonian leech, *Haementeria ghiliani* (Condra *et al.*, 1989; Blankenship *et al.*, 1990; Brankamp *et al.*, 1990); hirustasin was identified in the salivary glands of the European medicinal leech, *Hirudo medicinalis* (Söllner *et al.*, 1994). The latter protein is an inhibitor of tissue kallikrein, trypsin and chymotrypsin, but it does not inhibit factor Xa.

Alignment of the 20 cysteines present in antistasin reveals a 2-fold internal repeat, suggesting that the protein has evolved via gene duplication (Nutt *et al.*, 1988). The two repeats are very similar: the N-terminal domain (amino acid residues 1–55) and the C-terminal domain (amino acid residues 56–119) display ~40% identity and ~56% homology in their amino acid sequences (Dunwiddie *et al.*, 1989). Between cysteines 82 and 88 in the C-terminal

© Oxford University Press

```
                                  Subdomain 1                    Subdomain 2

                                *     *     *       * *       *↓  *          *    * *
Antistasin Domain 1          1  EDPFGPGCEE AGCPEGSACN IITDRCTCSG    VRCRVHCPHG FQRSRYGCEF -CKCRL            55
Antistasin isoforms             QG  R                          E        M                    I
Ghilanten Domain 1                                             PE         Y S            V   R  T
Antistasin Domain 2         56   EPMKATCDI SECPEGMMCS RLTNKCDCKI   DINCRKTCPNG LKRDKLGCEY -CECRPKRKL IPRLS  119
Antistasin isoforms
Ghilanten Domain 2                                                                        K      V
Hirustasin                   1    TQGNTCGG ETCSAAQVC- -LKGKCVCNE    VHCRIRCKYG LKKDENGCEY PCSCAKASQ          55
```

Fig. 1. Amino acid sequences of antistasin-type inhibitors. The sequences of antistasin (Nutt *et al.*, 1988; Han *et al.*, 1989; Theunissen *et al.*, 1994), ghilanten (Blankenship *et al.*, 1990) and hirustasin (Söllner *et al.*, 1994) are aligned. For antistasin, the sequence of the recombinant protein, of which the structure is presently discussed, is given in the upper line. Underneath, amino acid substitutions with respect to this sequence are indicated for ghilanten and antistasin isoforms. Cysteines are highlighted by asterisks; a dash indicates a gap in the protein sequence. The position of the reactive site arginine is marked by an arrow.

domain, there is one insertion of a single amino acid residue compared with the corresponding cysteines in the N-terminal domain. Furthermore, the C-terminal domain has a nine-residue extension with four positively charged amino acids.

Mutation studies have shown that only the N-terminal domain of antistasin is necessary for the inhibition of factor Xa; the C-terminal domain does not contribute to its inhibitory activity (O'Neill Palladino *et al.*, 1991; Theunissen *et al.*, 1994). The reactive site of antistasin is formed by Arg34 (the P1-residue) and Val35 (the P1′-residue) in the N-terminal domain (Dunwiddie *et al.*, 1989). Factor Xa slowly cleaves the peptide bond between these residues. The C-terminal residues equivalent to Arg34 and Val35 are Arg89 and Lys90, respectively. A Lys90→Val substitution, however, did not restore the inhibitory activity towards factor Xa (Hofmann *et al.*, 1992; Theunissen *et al.*, 1994), indicating that there are other factors causing the inactivity of the C-terminal domain.

To investigate the mechanism of action of antistasin and the atomic details of its interaction with factor Xa, we initiated the crystal structure determination of antistasin. A preliminary crystallographic analysis has been published previously (Schreuder *et al.*, 1993). Here, we report the 3D-structure of antistasin at 1.9 Å resolution and suggest a model of the antistasin–factor Xa complex, based on the antistasin and factor Xa crystal structures. Our structural results indicate that antistasin uses reactive site as well as exosite interactions to bind to factor Xa.

Results

Electron density map and quality of the model

Table I summarizes the final results of the crystallographic refinement of antistasin. Two antistasin structures have been determined, one at room temperature (2.3 Å resolution) and one at 100 K to a resolution of 1.9 Å. A superposition of the two structures revealed root mean square (r.m.s.) differences for Cαs of 0.28 Å, a value close to the coordinate error of the two structures as determined from a Luzzati plot (not shown). The crystallographic *R*-factors are 19.4% and 21.7%, respectively, for the 2.3 Å and 1.9 Å structures. In both cases, the final model consists of amino acid residues 7–110. For the six N-terminal and the nine C-terminal residues, the density is too weak to define their positions with confidence. Residues 9–11, 94 and some side chains developed temperature factors of ~50 Å^2 and higher during refinement. These residues are disordered in the crystal structure. Several other amino acids, for example Phe50, Glu56, Ser65, Met71 and Arg75, may adopt two different conformations of which only the most prominent has been modelled. The overall geometry of both antistasin structures is good, as can be judged from the r.m.s. deviations from ideal geometry given in Table I and from the absence of outliers in the Ramachandran plot (not shown). The electron density map (Figure 2) is in good agreement with the published sequence and, in addition, establishes the so far unknown disulfide bond connectivities.

Overall structure

Figure 3 shows the 1.9 Å 3D-structure of antistasin as a simplified ribbon model. As could be expected on the basis of the internal sequence homology, antistasin consists of two structurally similar domains, the N-terminal domain (residues 1–55) and the C-terminal domain (residues 56–119), in agreement with the prediction of Nutt *et al.* (1988). The domains are spatially distant with no interdomain backbone–backbone interactions and only few side chain–main chain and side chain–side chain interactions. They can further be subdivided into four similarly sized subdomains, two in each domain. The subdomains are linked by two hinge regions, consisting of Val31 and Arg32 in the N-terminal domain, and Asp85, Ile86 and Asn87 in the C-terminal domain. Since the hinge is more open in the C-terminal domain, this domain adopts a flat shape, whereas the N-terminal domain is wedge-shaped (see Figure 4). The difference in linker angle is caused by the insertion of Asp85 and by the special ϕ,ψ angles of Gly30 (91° and 160°). In the C-terminal domain, the residue corresponding to Gly30 is an isoleucine. However, apart from the differences in the hinge regions, the individual subdomains superimpose very well, with r.m.s. differences of Cα atoms being only 0.60 Å for residues 33–55 and 88–110 and 0.77 Å for residues 13–30 and 67–84.

Folding pattern of the domains in antistasin

Antistasin appears to exhibit mainly random coil structure (see Figure 3). Although two short antiparallel β-strands can be identified in each of the two domains on the basis of ϕ,ψ angles (involving residues 41–43 and 49–53 in the N-terminal domain and residues 96–98 and 104–108

Table I. Refinement statistics

Temperature (K)	293	100
Resolution range (Å)	5.0–2.3	5.0–1.9
Reflections used [$F_o > 0\sigma(F_o)$]	5711	9103
Final *R*-factor (%)[a]	19.4	21.7
Average real-space correlation coefficient (%)		
σ_A-weighted ($2F_o - F_c$) map	0.91	0.91
σ_A-weighted ($2F_o - F_c$) OMIT map	0.86	0.87
Residues included	7–110	7–110
Number of non-H atoms		
Protein	790	790
Non-protein	62	89
R.m.s. deviations from ideality for bond lengths (Å)	0.012	0.015
R.m.s. deviations from ideality for bond angles (°)	2.53	1.49
Secondary structure analysis according to PROCHECK (Laskowski *et al.*, 1993)		
Residues in most favoured regions (%)	87.6	87.6
Residues in additional allowed regions (%)	12.4	12.4
Residues in generously allowed regions (%)	0.0	0.0
Residues in disallowed regions (%)	0.0	0.0
Average *B*-factors (Å^2)		
Protein atoms	29.5	25.5
Solvent	40.3	30.3
Protein Data Bank code		1SKZ

[a]*R*-factor = $(\Sigma||F_o|-|F_c||/\Sigma|F_o|)$.

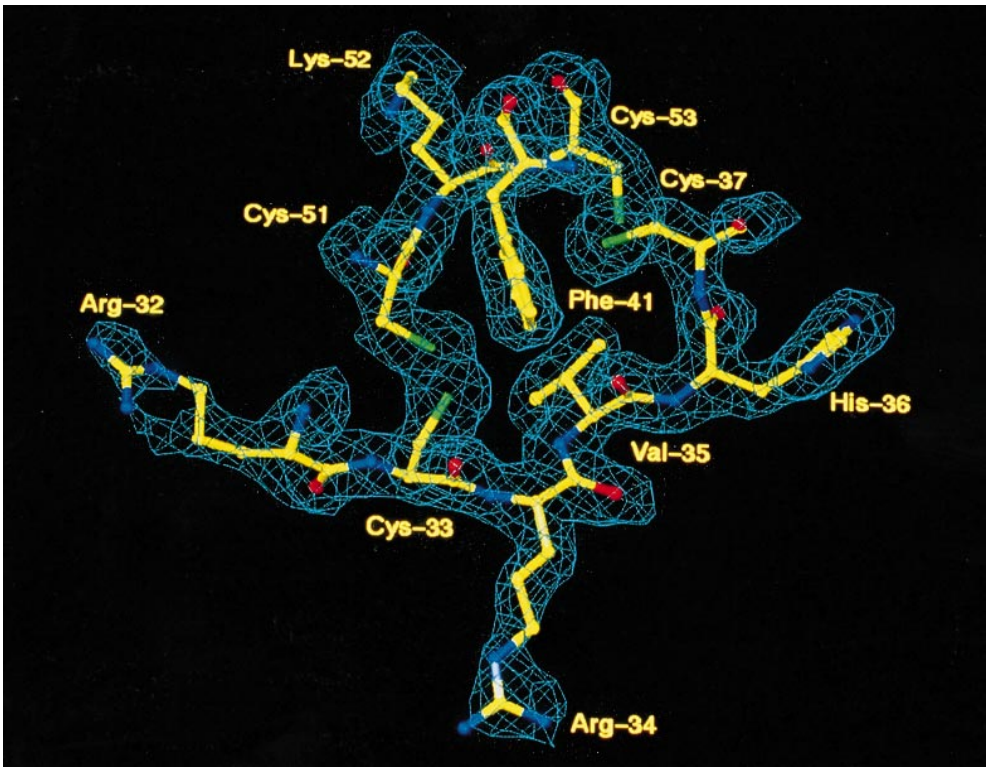

Fig. 2. Representative part of the σ_A-weighted (Read, 1986) ($2F_o$–F_c) OMIT map (Bhat, 1988; Vellieux and Dijkstra, 1997), centred at Arg34 and contoured at 1σ, showing the hydrophobic interaction network which stabilizes the reactive site loop of antistasin. Cysteines 33 and 51 and cysteines 37 and 53 are connected by disulfide bonds, respectively. The density for the side chain of Arg32 is somewhat weak. This residue is positioned close to a crystallographic 2-fold axis and has rather high B-values.

in the C-terminal domain, respectively), they lack the appropriate hydrogen bonding interactions and thus do not form real sheets. Also in the rest of the structure, main chain hydrogen bonding interactions are very limited. Instead, side chain contacts dominate the antistasin structure. There are no α-helices present in antistasin, only one single α-helical turn. This turn involves residues 8–11 and is positioned in a region with very high temperature factors. In addition, several reverse turns exist.

A remarkable feature of the antistasin structure is the absence of a proper core, which is also reflected by the fact that only 1144 Å^2 of the total accessible surface of antistasin (7394 Å^2) are buried. Instead, disulfide bridges seem to stabilize the fold. Antistasin contains 20 cysteine residues, 10 in each domain, all of which are involved in disulfide bridges. They are usually flanked by hydrophobic residues forming four small hydrophobic clusters, one in each subdomain, at topologically identical positions. In

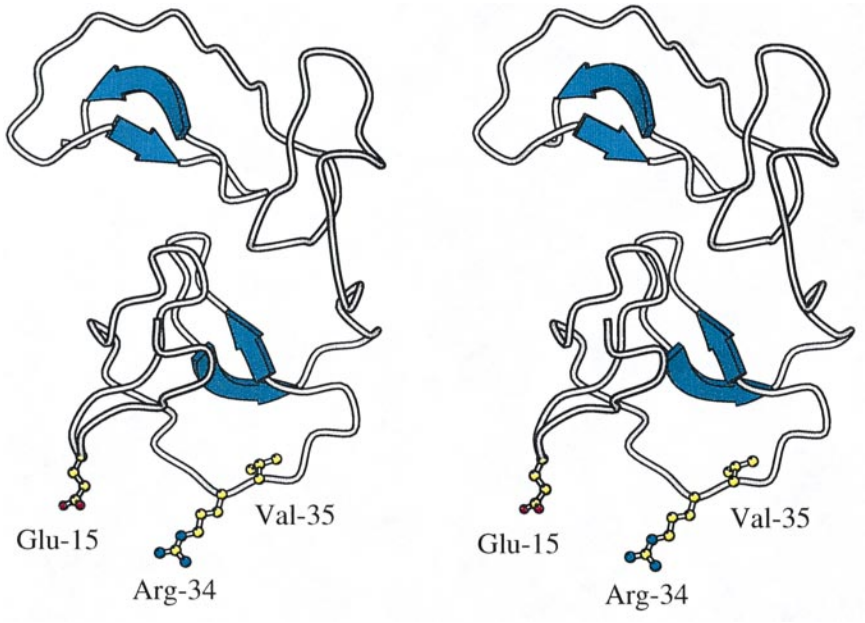

Fig. 3. Stereo view of the overall structure of antistasin from *H.officinalis* [produced with Molscript (Kraulis, 1991)]. The P1 and P1′ residues Arg34 and Val35, as well as Glu15 of the putative exosite binding region of antistasin are indicated.

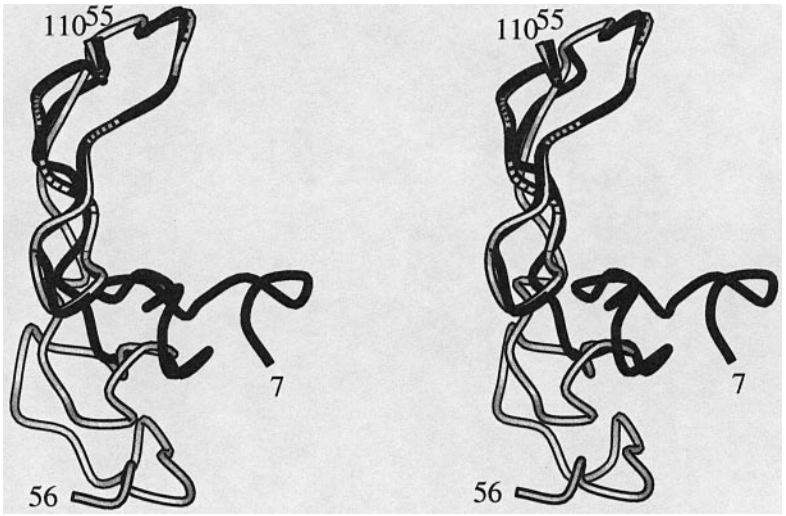

Fig. 4. Stereo view showing the superposition of the N- and C-terminal domains of antistasin, based on the Cα coordinates of the second subdomains, respectively [using the program O (Jones *et al.*, 1991); figure produced with Molscript (Kraulis, 1991)]. The N-terminal domain (black) adopts a wedge shape, while the C-terminal domain (grey) is relatively flat.

the N-terminal domain, disulfide bonds are observed between residues 8–19, 13–26, 28–48, 33–51 and 37–53 and in the C-terminal domain between residues 62–73, 67–80, 82–103, 88–106 and 92–108 (see Figure 5). Hence, all the disulfide bridges are within the individual domains, and two of them (involving Cys28/48 and Cys82/103) cross-bridge the subdomains.

The reactive site region

The reactive site of antistasin is formed by Arg34 (the P1-residue) and Val35 (the P1′-residue) in the N-terminal domain (Dunwiddie *et al.*, 1989). Arg34 is positioned at the tip of an exposed loop at the protein surface (see Figure 3). Its side chain has adopted an extended conformation. In the crystal, this residue is involved in contacts with a symmetry-related molecule. Val35 is pointing into the opposite direction. Compared with Arg34, the Val35 side chain is considerably less exposed. The reactive site loop is connected to the rest of the protein by two disulfide bonds involving Cys33 and Cys37 and is further stabilized by a network of hydrophobic interactions between these two disulfides and the Val31, Phe41 and Val35 side chains (see Figure 2). As a consequence of the various interactions, the temperature factors in the reactive site region are rather low, with values of ~15 Å^2 for most residues. For Cys33 and Arg34, temperature factors are somewhat higher, with values close to the average temperature factor of antistasin, which is 26 Å^2. Temperature factors are highest for Arg32 (up to 50 Å^2 for side chain atoms). Thus, although the reactive site loop is highly exposed, it has a well-defined conformation. Only the side chains of Arg32 and Arg34 are somewhat more flexible and may adapt their conformation to fit optimally into the active site of the target protease.

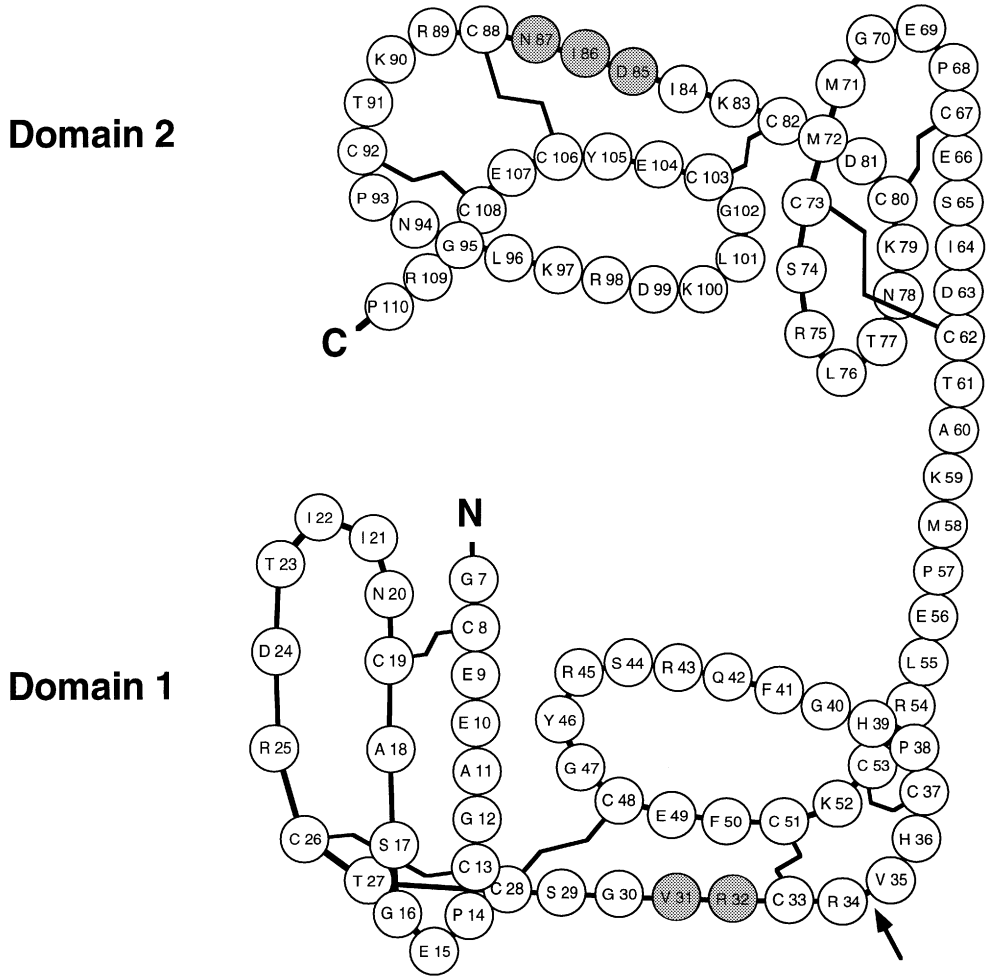

Fig. 5. Schematic representation of the antistasin fold. The orientation of antistasin is similar to the one chosen in Figure 3. Disulfide connectivities and the linker residues connecting the two subdomains within each domain are indicated. The scissile bond is marked by an arrow. β-strands involve amino acid residues 41–43 and 49–53 in the N-terminal domain and residues 96–98 and 104–108 in the C-terminal domain, respectively.

In the C-terminal domain of antistasin, the corresponding part of the reactive site (residues 87–92) also forms an exposed loop, positioned at the opposite end of the protein molecule. Its overall structure is very similar to the equivalent N-terminal region, as is reflected by the low r.m.s. differences in Cα positions of 0.43 Å for residues 88–92 compared with residues 33–37. As in the N-terminal domain, an arginine residue (Arg89) is at the position corresponding to P1, and also the network of hydrophobic interactions has a counterpart in the C-terminal domain, however, with Val31, Val35 and Phe41 being replaced by Ile86, the aliphatic part of the Lys90 side chain and Leu96, respectively.

Although the reactive site and its C-terminal counterpart appear very similar at first sight, some differences exist. Most obvious is the substitution of Val35 by Lys90. Other differences include a different side chain conformation of Arg89 compared with Arg34, the increased temperature factors for residues 90–97 compared with residues 35–42, and the differences in ϕ,ψ angles, especially for residues N-terminal of residue 88 and 33, respectively (see Table II).

Modelling of the factor Xa–antistasin complex

As we have not obtained crystals of a complex of antistasin with factor Xa, we performed docking studies in order to analyse possible binding modes of antistasin with its target protease. Antistasin was docked with its binding loop into the active site cleft of human factor Xa (Padmanabhan *et al.*, 1993; Brandstetter *et al.*, 1996) as described in Materials and methods (see Figure 6A). Docking was guided by the structures of the kallikrein A–BPTI (Chen and Bode, 1983) and trypsin–BPTI (Marquart *et al.*, 1983) complexes. Only the side chain of the P3 residue Arg32 had to be manually reoriented to optimize its fit in the active site. The resulting energy-minimized structure of antistasin exhibits r.m.s. differences for Cαs of 0.40 Å compared with the X-ray structure. For residues 32–39, r.m.s. differences are even smaller (0.35 Å), indicating that only minor changes were required for complex formation with factor Xa. Two major sites of antistasin were found to interact with factor Xa, consisting of residues 15–17 and 32–39, respectively. Additional contact zones may include the backbone carbonyl oxygen atoms of antistasin residues 8, 9 and 51, which are likely to interact with the side-chain amino groups of Lys148 and Lys96 of factor Xa, respectively. In the following, the two major interaction sites will be discussed in detail.

The reactive site region (residues 32–39). As in the uncomplexed structure of antistasin, the side chain of the

Table II. Main chain conformational angles ϕ,ψ of reactive site loops

	P3	P2	P1	P1′	P2′	P3′
Antistasin domain 1	Arg32	Cys33	Arg34	Val35	His36	Cys37
ϕ/ψ (°)	–93/39	–156/178	–129/29	–59/132	–71/112	–113/110
Antistasin domain 2	Asn87	Cys88	Arg89	Lys90	Thr91	Cys92
ϕ/ψ (°)	33/70	–125/125	–119/27	–77/146	–105/131	–136/138
Canonical values (from Bode and Huber, 1992)	140°<ϕ<–120°	–100°<ϕ<–60°	–120°<ϕ<–95°	–100°<ϕ<–60°	–140°<ϕ<–99°	–140°<ϕ<–99°
	140°<ψ<170° (except BPTI)	139°<ψ<180°	9°<ψ<50°	139°<ψ<180°	70°<ψ<120°	70°<ψ<120°

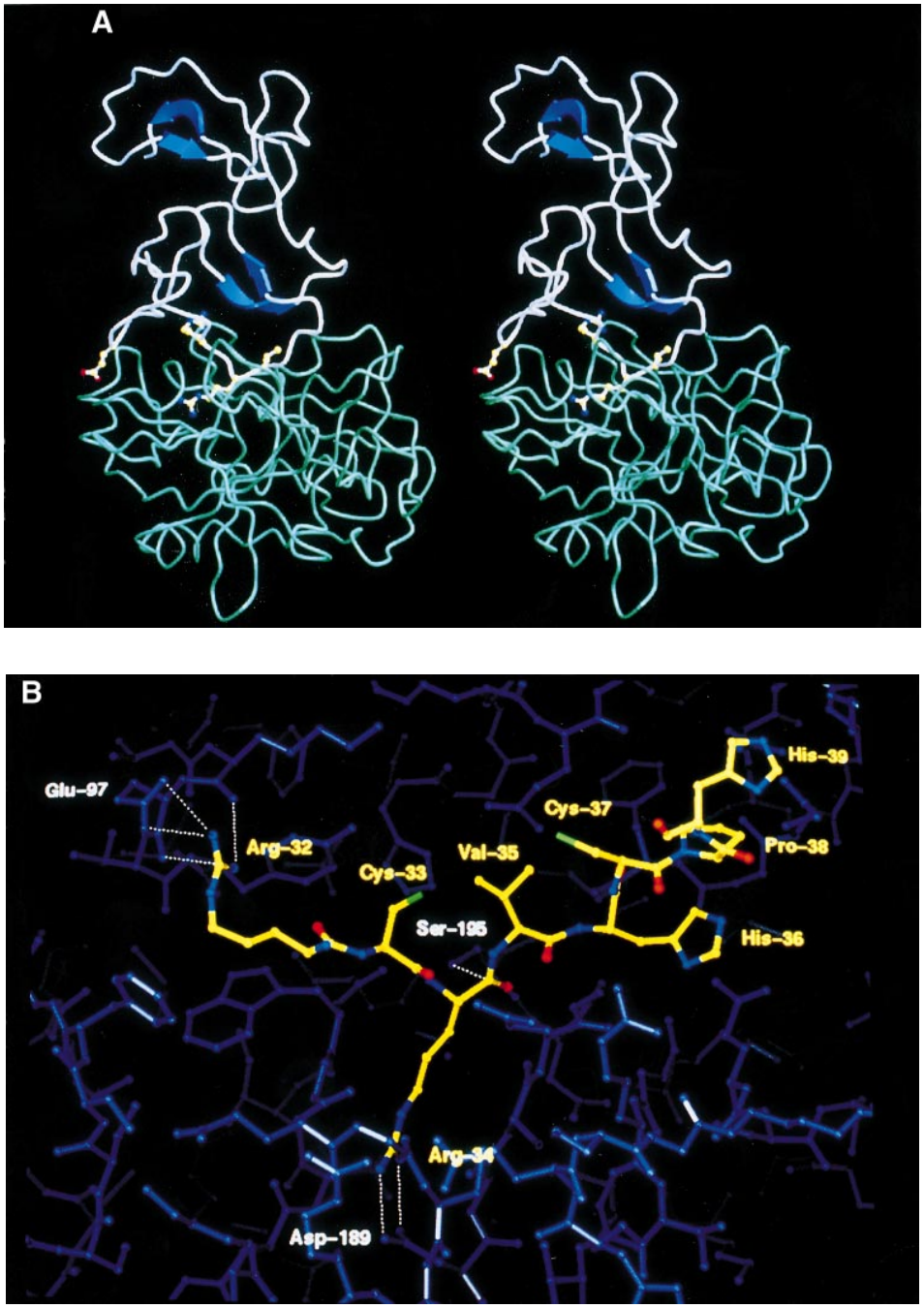

Fig. 6. Representative views of the modelled complex of antistasin and factor Xa. (**A**) Stereo view of the C_α trace [produced with Molscript (Kraulis, 1991) and Raster3D (Merritt and Murphy, 1994)]. Antistasin residues Glu15, Arg32 (P3), Arg34 (P1) and Val35 (P1′) are highlighted. (**B**) Reactive site area. Possible interactions of antistasin residues Arg32 and Arg34 with factor Xa are indicated. Ser195 of the factor Xa catalytic triad is perfectly positioned for nucleophilic attack by the protease.

P1 residue Arg34 adopts an extended conformation in the modelled complex with factor Xa. It forms a salt bridge with twin–twin geometry to Asp189 at the bottom of the S1 specificity pocket of factor Xa (see Figure 6B). The interaction is similar to that of Arg439 from a symmetry-related molecule in the native factor Xa crystal structure (Padmanabhan *et al.*, 1993). In addition to the ionic interactions, the Arg34 side chain is likely to be involved in hydrogen bonding interactions with the backbone carbonyl oxygen atoms of factor Xa residues 190, 216 and 218. The main chain carbonyl oxygen of Arg34 points into the oxyanion hole of factor Xa and probably forms hydrogen bonds with Ser195 N and Gly193 N. In the modelled complex, the scissile bond linking Arg34 and Val35 is sandwiched between the side chains of factor Xa residues Ser195 and Gln192, respectively, with the Arg34 carbonyl carbon being positioned only 2.9 Å from the serine Oγ of the factor Xa catalytic triad (His57, Asp102 and Ser195). This inhibitor atom thus seems perfectly positioned for nucleophilic attack by the protease.

The majority of serine proteases of the trypsin/chymotrypsin family form an antiparallel β-sheet with their substrates or inhibitors which involves residues 214–216 from the protease. However, in the modelled complex with antistasin, these residues seem not to contribute to hydrogen bonding interactions. This finding is in agreement with the results from Brandstetter *et al.* (1996) who determined the crystal structure of factor Xa with the synthetic inhibitor DX-9065a. The lack of β-sheet interactions is compensated for by two other major interactions between antistasin and factor Xa. One has already been described and involves the P1 residue Arg34. The second important interaction between antistasin and factor Xa concerns the P3 residue Arg32. In the modelled complex, the Arg32 guanidinium group binds to the cation hole of factor Xa, which is formed by the carbonyl oxygens of Lys96 and Glu97 as well as the Glu97 carboxylate (Brandstetter *et al.*, 1996) (see Figure 6B). The aliphatic part of the Arg32 side chain partly occupies the aryl binding site (S4) of factor Xa. The P4 residue Val31 is positioned far away from this binding site and seems not to interact with factor Xa. Thus, two residues, Arg32 and Arg34, are likely to be particularly important for the interaction of antistasin with factor Xa, with most of the interaction potential of the side chains of these residues satisfied.

The exosite binding region (residues 15–17). An unprecedented feature of the antistasin structure is the region comprising residues 15–17. In our model, the Glu15 side chain, which interacts with Arg25 from a symmetry-related molecule in the crystal structure, is reoriented towards a cluster of three positively charged residues, Arg222, Lys223 and Lys224, on the surface of factor Xa. We will refer to this contact area as the 'exosite'. Evidence exists that this putative exosite may not be unique for factor Xa, but may also be present in other proteases, since many factor Xa-related proteases like thrombin and trypsin also have positively charged amino acid residues at corresponding positions (Jackson and Nemerson, 1980). In addition to the charge–charge interactions, antistasin and factor Xa may form contacts via two hydrogen bonds involving the main chain carbonyl of Ser17 and the side chain of Arg222, respectively.

In view of the fact that only the N-terminal domain of antistasin can inhibit factor Xa, even though the C-terminal domain is highly homologous, it seemed very interesting also to perform docking studies of factor Xa with the C-terminal domain of antistasin. As a result, the inability of the C-terminal domain to inhibit factor Xa seems mainly to be caused by sites other than the region corresponding to the antistasin reactive site. Although at first sight, clashes of this part of antistasin with factor Xa seem inevitable, at second sight, they appear resolvable. For instance Arg89, which corresponds to the P1 residue, can easily reorient its side chain such that it adopts the same conformation as Arg34. And even Lys90, a residue much longer than the equivalent Val35 (P1′), can probably be accommodated into the corresponding factor Xa pocket. Much more serious are the clashes observed between antistasin residues Asn87 and, to a lesser extent, Asp85 with residues Trp215 and Phe174 of factor Xa, respectively. These two residues are positioned in the linker peptide which connects the two subdomains of the antistasin C-terminal domain. Another important difference to the modelled complex of factor Xa with the N-terminal domain of antistasin is the absence of the exosite interactions. Even though the residue corresponding to Glu15 is also conserved in the C-terminal domain of antistasin, it is positioned ~10 Å away from the corresponding position in the N-terminal domain, due to the different arrangement of subdomains in the two antistasin domains. In its position in the C-terminal domain, Glu69 cannot interact with factor Xa. Hence, although the C-terminal equivalent of the reactive site loop does not differ that much from its N-terminal counterpart, proper interaction with factor Xa is prevented by steric hindrance of the linker peptide and the absence of the exosite interactions.

Discussion

The antistasin structure and comparison with other protease inhibitors

Antistasin consists of two structurally similar domains both of which are mainly stabilized by five intra-domain disulfide bridges at topologically identical positions. Other protease inhibitors have been described, which are similarly rich in disulfide bridges, and also lack extensive secondary structural elements, such as squash seed inhibitor-I (Bode *et al.*, 1989) or mucous proteinase inhibitor (Grütter *et al.*, 1988). However, a more detailed comparison of the various structures, including a DALI search (Holm and Sander, 1993), revealed that only the protein hirustasin exhibits significant structural homology with antistasin. The structure of hirustasin was published, in complex with kallikrein (Mittl *et al.*, 1997), when finalizing this manuscript. Hirustasin is a related 55-residue protease inhibitor which shares 29% sequence identity with the N-terminal domain of antistasin and 38% with its C-terminal domain. It has a fold similar to the individual domains of antistasin and also has the same disulfide connectivity. As could be expected from the degree of sequence homology, hirustasin resembles the structure of the flat C-terminal domain rather than that of the wedge-shaped N-terminal domain of antistasin. However, hirustasin comprises two additional short, antiparallel β-strands in the first subdomain and also exhibits

a different relative orientation of the two subdomains compared with antistasin.

On the basis of a sequence alignment, the individual domains of antistasin were expected also to share a similar fold with decorsin and hirudin (Krezel *et al.*, 1994). Although the sequence alignment has ultimately proven incorrect (Mittl *et al.*, 1997), cysteine residues 8, 13, 19 and 26 of the first subdomain of the antistasin N-terminal domain do superimpose with the corresponding cysteines 17, 22, 27 and 38 of decorsin. In fact, r.m.s. differences for the cysteine Cα positions are only 0.27 Å and also the disulfide connectivity is the same. For the C-terminal domain of antistasin, the superposition is somewhat worse (r.m.s.d. = 1.1 Å). However, the spacing of the cysteine residues is different in the two structures and the loops connecting the cysteine residues do not superimpose. Similar results are found for a superposition with the corresponding cysteines of hirudin, although here the superposition of the connecting loops is somewhat better. Thus, although the overall structures of decorsin and hirudin differ from the antistasin and hirustasin structures, respectively, they do exhibit highly conserved elements.

Comparison of the N- and C-terminal domains of antistasin

The presence of 2-fold symmetry in the antistasin structure raises the possibility that this protein is a so-called 'multiheaded' inhibitor, similar to members of the Bowman–Birk, Kunitz and Kazal inhibitor families (reviewed by Laskowski and Kato, 1980). These proteins accommodate more than one reactive site. In contrast, the inhibitory activity of antistasin seems to be limited to its N-terminal domain, with only the peptide bond between Arg34 and Val35 being cleaved by factor Xa (Dunwiddie *et al.*, 1989; O'Neill Palladino *et al.*, 1991; Theunissen *et al.*, 1994). The absence of inhibitory activity of the C-terminal domain seems to be caused mainly by the overall shape of this domain. While in the N-terminal domain Arg32 (P3) is involved in an important contact with factor Xa, the corresponding residue in the C-terminal domain, Asn87 and, to a somewhat lesser extent also Asp85, exhibit serious clashes with factor Xa. Furthermore, the different positioning of the two subdomains prevents the interactions of the C-terminal domain of antistasin with the putative exosite of factor Xa. Thus, structural reasons clearly indicate why only the N-terminal and not the C-terminal domain of antistasin exhibits inhibitory activity against factor Xa. However, from our results it cannot be excluded that an as yet unidentified protease is inhibited by the antistasin C-terminal domain.

Reactive site

The reactive site [Arg34 (P1) and Val35 (P1′)] is positioned in an exposed loop which is connected to the rest of the protein by two disulfide bonds involving Cys33 and Cys37. Removal of one of the disulfide bonds by mutating Cys33 to glycine had no dramatic effect on the inhibitory activity of antistasin (Theunissen *et al.*, 1994), suggesting that Cys33 is not essential for activity. In the crystal structure, the two disulfides contribute to a tight hydrophobic interaction network involving also Val31, Phe41 and Val35. The disulfides thus clearly contribute to the stability of the reactive site loop. However, it is tempting to speculate that the disulfides might have an additional function. By covalently attaching the reactive site region to Cys51 and Cys53, two closely linked residues, the disulfide bonds could prevent the two peptide chains from moving too far apart after cleavage of the scissile bond, thus facilitating re-formation of the peptide bond. In this way, factor Xa would be inhibited by antistasin in a reversible manner, as has been observed by Dunwiddie *et al.* (1992b).

Interaction of antistasin with factor Xa

Why is antistasin such a potent (sub-nanomolar) factor Xa inhibitor? The results of structure determination and docking studies suggest that the interactions between factor Xa and antistasin involve two sites of factor Xa, the active site and an exosite. The reactive site loop of antistasin is suited for binding to the active site binding pockets of factor Xa, with the strongest interactions most likely involving the S1 pocket and the cation hole of factor Xa and the P1 and P3 residues of antistasin, respectively (Figure 6B). In addition, the region around antistasin residue Glu15 seems to be ideally positioned to interact with a cluster of positively charged residues on the factor Xa surface (residues 222–224). A multi-site binding that includes spatially remote sites is thermodynamically favourable because the total loss of entropy upon complexation 'has already been paid for' during the first interaction.

Implications for other factor Xa inhibitors

In the antistasin-like serine protease inhibitor hirustasin, the spacing of the ten cysteines is nearly identical to that in antistasin (see Figure 1) and also the disulfide connectivity is consistent (Mittl *et al.*, 1997). Hirustasin inhibits tissue kallikrein, trypsin, chymotrypsin and neutrophil cathepsin G, but it does not inhibit factor Xa. Why is this so? Of the eight amino acid residues in the P5–P3′ region of hirustasin, five residues are identical to those in antistasin and ghilanten isoforms (Nutt *et al.*, 1988; Blankenship *et al.*, 1990). Residues Arg32, Val35 and His36 of antistasin are replaced by histidine, isoleucine and arginine, respectively, in hirustasin. In our docking studies, Arg32 (P3) has been found to be involved in one of the most important interactions with factor Xa. It binds to the cation hole of factor Xa which is formed by the carbonyl oxygens of Lys96 and Glu97 as well as the Glu97 carboxylate. A histidine residue is much smaller than an arginine and would not reach into the cation hole unless factor Xa would undergo a structural change. Furthermore, the putative exosite interaction of Glu15 in the first domain of antistasin with the Arg222/Lys223/Lys224 cluster in factor Xa is not possible in hirustasin, since the corresponding amino acid residue in hirustasin is an alanine (Söllner *et al.*, 1994) (Figure 1). Antistasin and ghilanten isoforms, which all inhibit factor Xa, all have a glutamate residue at this position.

In the crystal structure of the hirustasin–kallikrein complex (Mittl *et al.*, 1997), the most important interactions between inhibitor and protease are found to involve the P1 and the P4 residues, rather than P1 and P3 as for antistasin. Even though the P4 residue is a valine in hirustasin as well as in antistasin, this residue has a different function in the two proteins. While in antistasin Val31 is involved in a tight hydrophobic interaction

Table III. Data collection and phasing statistics

Data set	Resolution (Å)	Measured reflections	Unique reflections	R_{merge} (%)	Completeness (%)	No. of sites	R_{deriv}	R_{Cullis}	Phasing power
Native 1	2.8	10608	3295	6.0	93				
Native 2	2.3	51863	6384	6.8	100				
Native 3[a]	1.9	100326	10300	8.0	95				
K_2PtCl_4-1	2.8	11710	3363	7.2	95	2	0.21	0.71	1.33
K_2PtCl_4-2	2.8	9197	3133	6.0	90	2	0.23	0.65	1.46
PIP	2.8	12026	3430	4.2	97	3	0.32	0.62	0.99
UO_2-acetate	3.2	8896	1672	7.2	67	4	0.13	0.68	0.96

$R_{merge} = \Sigma_h \Sigma_i |I(h)_i - <I(h)>| / \Sigma_h <I(h)>$, where $I(h)_i$ are the intensity measurements for a reflection and $<I(h)>$ is the mean intensity for this reflection.
$R_{deriv} = \Sigma_h |F_{PH} - F_P| / \Sigma_h |F_P|$, where F_{PH} and F_P are the structure factor amplitudes of the derivative and native crystals, respectively.
$R_{Cullis} = \Sigma_h ||F_{PH} \pm F_P| - F_H(calc)| / \Sigma_h |F_{PH} - F_P|$, where F_{PH} and F_P are defined as above, and $F_H(calc)$ is the calculated heavy atom structure factor amplitude summed over centric reflections only.
Phasing power = $<F_H>$/E, the r.m.s. heavy atom structure factor amplitude divided by the lack of closure error.
PIP = di-imul-iodobis(ethylenediamine)-di-platinum(II)-nitrate.
[a]The data set native 3 was obtained by scaling a 90% complete 1.9 Å data set collected at DESY (R_{sym} = 3.8%) to a 2.5 Å data set collected in house, also at cryogenic temperature.

network, which stabilizes the reactive site loop, the corresponding Val27 of hirustasin adopts an exposed position at the protein surface suited for a strong interaction with kallikrein. Hence, although the structures of antistasin and hirustasin are similar, the existing differences account for highly specific interactions with the target proteases.

Conclusion

The X-ray structure of antistasin reveals a novel folding motif of a protease inhibitor which consists of two domains, each resembling the structure of hirustasin. Antistasin predominantly consists of random coil structure, stabilized by ten disulfide bonds. The modelled factor Xa–antistasin complex suggests at least two interaction sites of the inhibitor with the target protease. These two sites are presumably essential for the inhibitor's specificity and binding affinity. At present we are investigating the relative importance of these interaction sites by mutational analysis inspired by the modelled complex of factor Xa and antistasin. In addition, the modelled complex is used for the design of novel low-molecular weight inhibitors.

Materials and methods

Antistasin preparation, crystallization and data collection

Recombinant antistasin, produced in Chinese hamster ovary cells, was prepared and crystallized with ammonium sulfate and sodium chloride as precipitants as described before (Schreuder *et al.*, 1993; Theunissen *et al.*, 1994). Antistasin crystallizes in space group *I*422 with cell dimensions $a = b = 78.3$ Å and $c = 88.5$ Å. The crystals contain one protein molecule per asymmetric unit. Heavy-atom derivatives were prepared by soaking crystals in 0.2 mM K_2PtCl_4 (1 day), 5 mM di-imul-iodobis(ethylenediamine)-di-platinum(II)-nitrate (2 days) or 10 mM uranyl acetate (5 days). For cryo experiments, antistasin crystals were pre-equilibrated for 2 days against a reservoir containing 30% ammonium sulfate, 2.2 M sodium chloride, 100 mM sodium citrate buffer, pH 6.0 and 20% glycerol. Crystals were then transferred to this solution, in which they were stable for at least 2 weeks, before actually performing the cryo experiments. Upon flash-freezing, the cell parameters of the antistasin crystals shrank to $a = b = 76.5$ Å and $c = 86.6$ Å.

Native and derivative data were collected on a FAST area detector mounted on a rotating anode X-ray generator operated at 40 kV and 80 mA. In addition, two higher-resolution native data sets were collected at synchrotron radiation sources, one at room temperature (native 2) and one at cryogenic temperature (native 3). The 2.3 Å room temperature data set was collected on beam line 9.7 at the SRS, Daresbury Laboratory, while the 1.9 Å cryo data set was collected on beam line BW7A at the EMBL outstation at DESY. Both beam lines were equipped with MAR image plate detectors. Data were processed using the BIOMOL (Groningen, NL) and CCP4 (Daresbury, UK) suites as well as XDS (Kabsch, 1988a,b, 1993). Details of data collection are given in Table III.

Phasing

The heavy-atom sites of the platinum derivatives could be located by inspection of the Harker sections of difference Patterson maps and by performing vector search calculations. The power of the derivatives was limited because of common sites. The binding sites of the uranyl derivative were found from difference Fouriers. The occupancy of these sites was unfortunately very low. After refinement of the heavy-atom parameters using PHARE (Bricogne, 1976), the overall figure of merit to 3.5 Å resolution was 0.56. Table III summarizes the phasing statistics.

Model building and refinement

The quality of the initial MIR map calculated at 3.5 Å resolution was poor, but some polypeptide chains could be built into it. Several cycles of constrained and restrained refinement with phase combination with the MIR phases and model building using FRODO (Jones, 1985) improved both the model and the map considerably and the chain could be traced, except for some N- and C-terminal residues. Crystallographic refinement was done using RESTRAIN (Driessen *et al.*, 1989) and X-PLOR (Brünger *et al.*, 1987). Refinement of the room temperature model of antistasin at 2.3 Å resolution resulted in an *R*-factor of 19.2% and a free *R*-factor of 26.4%. The last refinement cycle was repeated for all reflections including the test set, giving a final *R*-factor of 19.4%. The final model of the antistasin structure at room temperature consists of amino acid residues 7–110 and includes 62 water molecules. Subsequently, this structure without the water molecules was taken as the starting model for refinement of the cryo structure of antistasin. After rigid-body refinement, the *R*-factor was 36.8%. Seven rounds of refinement using X-PLOR and subsequent manual rebuilding of the model using O (Jones *et al.*, 1991), resulted in a final *R*-factor of 21.5% and a free *R*-factor of 27.4%. The corresponding *R*-factors at 2.3 Å resolution are 19.5% and 26.2%, respectively. The last refinement cycle was repeated with all the data including the test set and resulted in a structure with good stereochemistry and an *R*-factor of 21.7%. The final model at cryogenic temperature includes amino acids 7–110, 88 water molecules and one chloride ion. Refinement statistics are summarized in Table I. Coordinates and structure factors have been submitted to the Protein Data Bank under accession code 1SKZ.

Modelling the interaction of antistasin with factor Xa

All molecular modelling studies were carried out with Quanta/CHARMm 96 (MSI, San Diego). The all atom force field was used for factor Xa (4469 atoms) and antistasin (1536 atoms). The N- and C-termini were charged by applying default patches. Coordinates of human factor Xa in complex with the inhibitor DX-9065a were kindly provided to us by Dr Richard Engh (Max-Planck-Institut für Biochemie, Martinsried). Docking of the antistasin binding loop onto the active site cleft of factor Xa was guided by the structures of the kallikrein A–BPTI [PDB entry

2KAI (Chen and Bode, 1983)] and trypsin–BPTI [PDB entry 2PTC (Marquart *et al*., 1983)] complexes, assuming that the relative position and orientation of the binding loops and the active sites in all these complexes are similar. Only the side chain of the P3 residue Arg32 had to be manually reoriented to optimize its fit in the active site. In the antistasin crystal structure, any other than the observed conformation of Arg32 would lead to clashes with a symmetry-related molecule. Energy minimizations were carried out using the Newton–Raphson algorithm until the r.m.s. value of the energy gradient was <0.2 kcal/mol·Å. Initially, only the residues in the contact zone were energy-minimized, while the rest of the system was kept fixed. In a second step, the whole system was energy-minimized without applying constraints. During energy minimization, the electrostatics were scaled down by using a distance-dependent dielectric function of $\varepsilon = 2R$ (Grootenhuis and van Galen, 1995). Switching and shifting functions were turned on for distances up to 11 and 14 Å for the van der Waals and electrostatic interactions, respectively.

Acknowledgements

R.L. thanks the European Molecular Biology Organisation for a long-term fellowship. Additional financial support was received from the European Union for the work at EMBL Hamburg through the HCMP Access to Large Installations Project, contract No. CHGE-CT93-0040. The authors gratefully acknowledge the excellent technical assistance of Joop Swinkels and Toon van der Doelen. Piet Levering, Anjo van Heijst and Leontien den Hoed are thanked for the large-scale cell culture of recombinant antistasin. We appreciate Arie Visser's valuable comments on the putative exosite on factor Xa.

References

Bhat,T.N. (1988) Calculation of an OMIT map. *J. Appl. Crystallogr.*, **21**, 279–281.

Blankenship,D.T., Brankamp,R.G., Manley,G.D. and Cardin,A.D. (1990) Amino acid sequence of ghilanten: anticoagulant-antimetastatic principle of the South American leech, *Haementeria ghilianii*. *Biochem. Biophys. Res. Commun.*, **166**, 1384–1389.

Bode,W. and Huber,R. (1992) Natural protein proteinase inhibitors and their interaction with proteinases. *Eur. J. Biochem.*, **204**, 433–451.

Bode,W., Greyling,H.J., Huber,R., Otlewski,J. and Wilusz,T. (1989) The refined 2.0 Å X-ray crystal structure of the complex formed between bovine β-trypsin and CMTI-I, a trypsin inhibitor from squash seeds (*Cucurbita maxima*). *FEBS Lett.*, **242**, 285–292.

Brandstetter,H., Kühne,A., Bode,W., Huber,R., von der Saal,W., Wirthensohn,K. and Engh,R.A. (1996) X-ray structure of active site-inhibited clotting factor Xa. *J. Biol. Chem.*, **271**, 29988–29992.

Brankamp,R.G., Blankenship,D.T., Sunkara,P.S. and Cardin,A.D. (1990) Ghilantens: anticoagulant-antimetastatic proteins from the South American leech, *Haementeria ghilianii*. *J. Lab. Clin. Med.*, **115**, 89–97.

Bricogne,G. (1976) Methods and programs for direct-space exploitation of geometric redundancies. *Acta Crystallogr.*, **A32**, 832–847.

Brünger,A.T., Kuriyan,J. and Karplus,M. (1987) Crystallographic R-factor refinement by molecular dynamics. *Science*, **235**, 458–460.

Chen,Z. and Bode,W. (1983) Refined 2.5 Å X-ray crystal structure of the complex formed by porcine kallikrein A and the bovine pancreatic trypsin inhibitor. Crystallization, Patterson search, structure determination, refinement, structure and comparison with its components and with the bovine trypsin-pancreatic trypsin inhibitor complex. *J. Mol. Biol*., **164**, 283–311.

Condra,C., Nutt,E.M., Petroski,C.J., Simpson,E., Friedman,P.A. and Jacobs,J.W. (1989) Isolation and structural characterization of a potent inhibitor of coagulation factor Xa from the leech, *Haementeria ghilianii*. *Thromb. Haemost.*, **61**, 437–441.

Driessen,H., Haneef,M.I.J., Harris,G.W., Howlin,B., Khan,G. and Moss,D.S. (1989) RESTRAIN: restrained structure-factor least-squares refinement program for macromolecular structures. *J. Appl. Crystallogr.*, **22**, 510–516.

Dunwiddie,C., Thornberry,N.A., Bull,H.G., Sardana,M., Friedman,P.A., Jacobs,J.W. and Simpson,E. (1989) Antistasin, a leech-derived inhibitor of factor Xa. *J. Biol. Chem.*, **264**, 16694–16699.

Dunwiddie,C.T., Nutt,E.M., Vlasuk,G.P., Siegl,P.K.S. and Schaffer,L.W. (1992a) Anticoagulant efficacy and immunogenicity of the selective factor Xa inhibitor antistasin following subcutaneous administration in the Rhesus monkey. *Thromb. Haemost.*, **67**, 371–376.

Dunwiddie,C.T., Vlasuk,G.P. and Nutt,E.M. (1992b) The hydrolysis and resynthesis of a single reactive site peptide bond in recombinant antistasin by coagulation factor Xa. *Arch. Biochem. Biophys.*, **294**, 647–653.

Grootenhuis,P.D.J. and van Galen,P.J.M. (1995) Correlation of binding affinities with non-bonded interaction energies of thrombin-inhibitor complexes. *Acta Crystallogr.*, **D51**, 560–566.

Grütter,M.G., Fendrich,G., Huber,R. and Bode,W. (1988) The 2.5 Å X-ray crystal structure of the acid-stable proteinase inhibitor from human mucous secretions analysed in its complex with bovine α-chymotrypsin. *EMBO J.*, **7**, 345–351.

Han,J.H. *et al*. (1989) Cloning and expression of cDNA encoding antistasin, a leech-derived protein having anti-coagulant and anti-metastatic properties. *Gene*, **75**, 47–57.

Hauptmann,J. and Kaiser,B. (1993) Anticoagulant and antithrombotic action of the Factor Xa inhibitor antistasin (ATS). *Thromb. Res.*, **71**, 169–174.

Hofmann,K.J., Nutt,E.M. and Dunwiddie,C.T. (1992) Site-directed mutagenesis of the leech-derived Factor Xa inhibitor antistasin. *Biochem. J.*, **287**, 943–949.

Holm,L. and Sander,C. (1993) Protein structure comparison by alignment of distance matrices. *J. Mol. Biol.*, **233**, 123–138.

Jackson,C.M. and Nemerson,Y. (1980) Blood coagulation. *Annu. Rev. Biochem.*, **49**, 765–811.

Jones,T.A. (1985) Interactive computer graphics: FRODO. *Methods Enzymol.*, **115**, 157–171.

Jones,T.A., Zou,J.-Y., Cowan,S.W. and Kjelgaard,M. (1991) Improved methods for building protein models in electron density maps and the location of errors in these maps. *Acta Crystallogr.*, **A47**, 110–119.

Kabsch,W. (1988a) Automatic indexing of rotation diffraction patterns. *J. Appl. Crystallogr.*, **21**, 67–71.

Kabsch,W. (1988b) Evaluation of single-crystal X-ray diffraction data from a position-sensitive detector. *J. Appl. Crystallogr.*, **21**, 916–924.

Kabsch,W. (1993) Automatic processing of rotation diffraction data from crystals of initially unknown symmetry and cell constants. *J. Appl. Crystallogr.*, **26**, 795–800.

Kraulis,P.J. (1991) MOLSCRIPT: a program to produce both detailed and schematic plots of protein structures. *J. Appl. Crystallogr.*, **24**, 946–950.

Krezel,A.M., Wagner,G., Seymour-Ulmer,J. and Lazarus,R.A. (1994) Structure of RGD protein decorsin: conserved motif and distinct function in leech proteins that affect blood clotting. *Science*, **264**, 1944–1947.

Laskowski,M.,Jr and Kato,I. (1980) Protein inhibitors of proteinases. *Annu. Rev. Biochem.*, **49**, 593–626.

Laskowski,R.A., MacArthur,M.W., Moss,D.S. and Thornton,J.M. (1993) PROCHECK: a program to check the stereochemical quality of protein structures. *J. Appl. Crystallogr.*, **26**, 283–291.

Mao,S.S. (1993) Factor Xa inhibitors. *Perspect. Drug Discov. Design*, **1**, 423–430.

Marquart,M., Walter,J., Deisenhofer,J., Bode,W. and Huber,R. (1983) The geometry of the reactive site and of the peptide groups in trypsin, trypsinogen and its complexes with inhibitors. *Acta Crystallogr.*, **B39**, 480–490.

Mellott,M.J., Holahan,M.A., Lynch,J.J., Vlasuk,G.P. and Dunwiddie,C.T. (1992) Acceleration of recombinant tissue-type plasminogen activator-induced reperfusion and prevention of reocclusion by recombinant antistasin, a selective Factor Xa inhibitor, in a canine model of femoral arterial thrombosis. *Circ. Res.*, **70**, 1152–1160.

Merritt,E.A. and Murphy,M.E.P. (1994) Raster3D version 2.0, a program for photorealistic molecular graphics. *Acta Crystallogr.*, **D50**, 869–873.

Mittl,P.R.E., Di Marco,S., Fendrich,G., Pohlig,G., Heim,J., Sommerhoff,C., Fritz,H., Priestle,J.P. and Grütter,M.G. (1997) A new structural class of serine protease inhibitors revealed by the structure of the hirustasin-kallikrein complex. *Structure*, **5**, 253–264.

Nutt,E., Gasic,T., Rodkey,J., Gasic,G.J., Jacobs,J.W., Friedman,P.A. and Simpson,E. (1988) The amino acid sequence of antistasin. *J. Biol. Chem.*, **263**, 10162–10167.

Nutt,E.M., Jain,D., Lenny,A.B., Schaffer,L., Siegl,P.K. and Dunwiddie, C.T. (1991) Purification and characterization of recombinant antistasin: a leech-derived inhibitor of coagulation Factor Xa. *Arch. Biochem. Biophys.*, **285**, 37–44.

O'Neill Palladino,L. *et al*. (1991) Expression and characterization of the N-terminal half of antistasin, an anticoagulant protein derived from the leech *Haementeria officinalis*. *Protein Expr. Purif.*, **2**, 37–42.

Padmanabhan,K., Padmanabhan,K.P., Tulinsky,A., Park,C.H., Bode,W., Huber,R., Blankenship,D.T., Cardin,A.D. and Kisiel,W. (1993) Structure of human des(1-45) factor Xa at 2.2 Å resolution. *J. Mol. Biol.*, **232**, 947–966.

Read,R.J. (1986) Improved Fourier coefficients for maps using phases from partial structures with errors. *Acta Crystallogr.*, **A42**, 140–149.

Schreuder,H., Arkema,A., de Boer,B., Kalk,K., Dijkema,R., Mulders,J., Theunissen,H. and Hol,W. (1993) Crystallization and preliminary crystallographic analysis of antistasin, a leech-derived inhibitor of blood coagulation Factor Xa. *J. Mol. Biol.*, **231**, 1137–1138.

Söllner,C., Mentele,R., Eckerskorn,C., Fritz,H. and Sommerhof,C.P. (1994) Isolation and characterization of hirustasin, an antistasin-type serine protease inhibitor from the medical leech *Hirudo medicinalis*. *Eur. J. Biochem.*, **219**, 937–943.

Theunissen,H.J.M., Dijkema,R., Swinkels,J.C., de Poorter,T.L., Vink,P.M.F. and van Dinther,T.G. (1994) Mutational analysis of antistasin, an inhibitor of blood coagulation Factor Xa derived from the Mexican leech *Haementeria officinalis*. *Thromb. Res.*, **75**, 41–50.

Tuszinsky,G.P., Gasic,T.B. and Gasic,G.J. (1987) Isolation and characterization of antistasin: an inhibitor of metastasis and coagulation. *J. Biol. Chem.*, **262**, 9718–9723.

Vellieux,F.M.D. and Dijkstra,B.W. (1997) Computation of Bhat's OMIT maps with several coefficients. *J. Appl. Crystallogr.*, **30**, 396–399.

Vlasuk,G.P., Ramjit,D., Fujita,T., Dunwiddie,C.T., Nutt,E.M., Smith,D.E. and Shebuski,R.J. (1991) Comparison of the *in vivo* anticoagulant properties of standard heparin and the highly selective Factor Xa inhibitors antistasin and tick anticoagulant peptide (TAP) in a rabbit model of venous thrombosis. *Thromb. Haemost.*, **65**, 257–262.

Received on April 20, 1997; *revised on June 12, 1997*